Unusual Binding Mode of the 2*S*4*R* Stereoisomer of the Potent Aldose Reductase Cyclic Imide Inhibitor Fidarestat (2*S*4*S*) in the 15 K Crystal Structure of the Ternary Complex Refined at 0.78 Å Resolution: Implications for the Inhibition Mechanism

Hai-Tao Zhao,[†] Isabelle Hazemann,[§] Andre Mitschler,[§] Vincenzo Carbone,[†] Andrzej Joachimiak,[‡] Steve Ginell,[‡] Alberto Podjarny,[§] and Ossama El-Kabbani*[,†]

Department of Medicinal Chemistry, Victorian College of Pharmacy, Monash University (Parkville Campus), 381 Royal Parade, Vic 3052, Australia, Departement de Biologie et Genomique Structurale, IGBMC, CNRS INSERM ULP, 1 rue Laurent Fries, B.P. 163, 67404 Illkirch, France, and Structural Biology Center, Biosciences Division, Argonne National Laboratory, Argonne, Illinois

Received December 5, 2007

The structure of human aldose reductase in complex with the 2*S*4*R* stereoisomer of the potent inhibitor Fidarestat ((2*S*,4*S*)-6-fluoro-2′,5′-dioxospiro-[chroman-4,4′-imidazoline]-2-carboxamide) was determined at 15 K and a resolution of 0.78 Å. The structure of the complex provides experimental evidence for the inhibition mechanism in which Fidarestat is initially bound neutral and then becomes negatively charged by donating the proton at the 1′-position nitrogen of the cyclic imide ring to the Nϵ2 atom of the catalytic His110.

Introduction

Aldose reductase (ALR2; EC 1.1.1.21) is a 36-kDa enzyme belonging to the aldo-keto reductase superfamily. It is the first and rate-determining enzyme of the polyol pathway of glucose metabolism that, in the presence of NADPH, converts glucose into sorbitol.[1,2] Glucose overutilization through the polyol pathway during hyperglycaemia has been linked to various tissue-based pathologies associated with diabetes complications, such as cataract formation, peripheral neuropathy, and diabetes-linked kidney lesions.[3–7] Thus, inhibition of ALR2 offers a potential treatment for the debilitating pathologies associated with chronic hyperglycaemia that occurs with diabetes mellitus. Many ALR2 inhibitors (ARIs) have been reported in the literature, however, due to lack of efficacy and unacceptable side effects, most drug candidates were not approved for clinical use. At present only Epalrestat, which was developed by Ono and launched into the Japanese market in 1992, is available for the treatment of diabetes complications. Several new potential candidates are currently in development, and are waiting for future approval to enter the drug market, which includes the promising cyclic imide inhibitor Fidarestat ((2*S*,4*S*)-6-fluoro-2′,5′-dioxospiro-[chroman-4,4′-imidazoline]-2-carboxamide).[8–11] Encouraging results obtained from clinical trials showed that Fidarestat inhibited structural and functional progressions of diabetic neuropathy as well as halted the increase in sorbitol pathway flux in diabetic patients.[12,13]

While experimental evidence for the neutral state of cyclic imide inhibitors when initially bound to the enzyme was not available prior to this study, the 0.92 Å resolution crystal structure of human aldose reductase holoenzyme in complex with Fidarestat showed an electrostatic interaction between a negatively charged 1′-position nitrogen atom of the cyclic imide ring and the Nϵ2 of the catalytic His110 (Scheme 1).[14] This finding explained the tight binding of the inhibitor and was supported by the fact that the translation from in vitro to in vivo activity for the compound was easily achieved.[15–17] In addition, previous determinations of human aldose reductase holoenzyme structures in complex with stereoisomers of Fidarestat at resolutions up to 1.3 Å suggested that the differences in the interactions between the cyclic imide rings and the exocyclic amide groups of the compounds with residues His110, Trp111, Trp219, and Cys298 account for the differences in their inhibitory potencies.[18]

Scheme 1

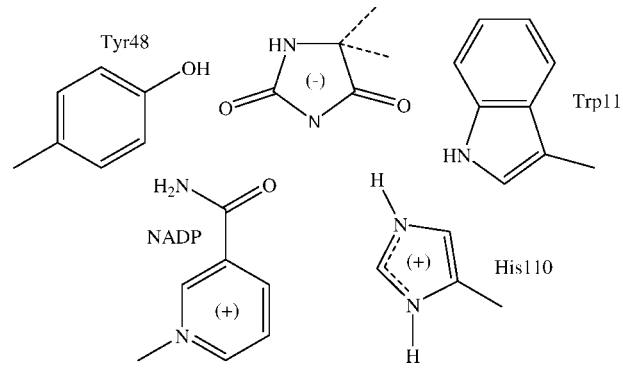

Scheme 2

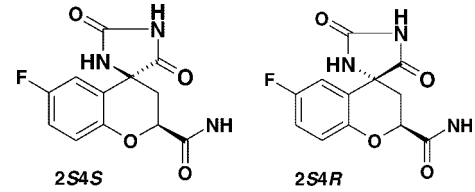

In this study we report the structure of ALR2 holoenzyme complexed with the 2*S*4*R* stereoisomer of Fidarestat (Scheme 2) determined with X-ray diffraction data collected at a temperature of 15 K and refined at 0.78 Å resolution. The ultrahigh resolution structure allowed for the determination of the protonation state of the inhibitor and provided experimental evidence for the hydrogen present at the 1′-position nitrogen atom in the cyclic imide ring of the inhibitor. These findings together with the 0.92 Å crystal structure of the ALR2−Fidarestat

* To whom correspondence should be addressed. Phone: 61-3-9903-9691. Fax: 61-3-9903-9582. E-mail: ossama.el-kabbani@vcp.monash.edu.au.
[†] Victorian College of Pharmacy.
[§] IGBMC, CNRS INSERM ULP.
[‡] Argonne National Laboratory.

10.1021/jm701514k CCC: $40.75
Published on Web 02/20/2008

Table 1. Data Collection and Refinement Statistics

Data Collection and Processing	
No. of crystals used	1
wavelength (Å)	0.9000
space group	$P2_1$
unit cell parameters	
a, b, c (Å)	49.20, 66.64, 47.28
α, β, γ (°)	90.00, 91.67, 90.00
Diffraction Data	
resolution range (Å)	99–0.78
unique reflections	336314
$R(I)_{merg}$ (overall)	2.7%
$R(I)_{merg}$[a]	12.3%
completeness (overall)	97.3%
completeness[a]	93.3%
redundancy (overall)	2.1
redundancy[a]	2.0
$I/\sigma(I)$ (overall)	16.69
$I/\sigma(I)$[a]	10.27
Refinement	
resolution range (Å)	10–0.78
reflections used in refinement (work/test)	319354/16809
R values for all reflections (work/test)	
isotropic refinement	
R_{cryst}/R_{free} without H (%)	19.66/20.76
anisotropic refinement	
R_{cryst}/R_{free} with H (%)	10.54/11.50
R_{cryst}/R_{free} without H (%)	12.54/13.08
reflections with $F > 4\sigma_F$ (work/test)	303890/15972
R values based on $F > 4\sigma_F$	
isotropic refinement	
R_{cryst}/R_{free} without H (%)	19.03/20.25
anisotropic refinement	
R_{cryst}/R_{free} with H (%)	10.06/11.00
R_{cryst}/R_{free} without H (%)	12.01/12.56
protein residues	316
coenzyme	1
inhibitor	1
citrate	1
water molecules	684
RMSDs	
bonds (Å)	0.018
angles (°)	2.3
dihedrals (°)	11.5
Ramachandran Plot	
residues in most favored regions	90.3%
residues in additional allowed regions	9.7%
Estimated Coordinated Error	
Luzzati mean error (Å)	0.031
Mean B Factor (Å^2)	
protein	10.00
$NADP^+$	4.11
inhibitor	4.26
citrate	6.40

[a] Data in the highest resolution shell (0.81–0.78 Å).

complex suggest a mechanism of ALR2 inhibition by cyclic imide compounds in which the Nϵ2 atom of the catalytic His110 accepts a proton from the 1′-position nitrogen atom of the cyclic imide ring after the inhibitor is bound resulting in a negatively charged inhibitor and a positively charged imidazole ring of His110, contributing to strong inhibitor binding.

Results and Discussion

Structure of the Ternary Complex. The structure of the holoenzyme in complex with the 2*S*4*R* stereoisomer of Fidarestat was determined at 0.78 Å resolution, with a final R_{cryst} of 10.06%, and R_{free} of 11.00% (Table 1). The asymmetric unit consisted of 316 amino acids, 1 $NADP^+$ coenzyme, 1 inhibitor, 1 citrate and 684 water molecules. Multiple conformations were observed for the side-chains of 69 amino acid residues. The Ramachandran Φ, Ψ plot of main-chain torsion angles placed 90.3% and 9.7% of the ALR2 residues in the most favored and additional allowed regions, respectively. The statistics for stereochemistry and geometry of the final model are shown in Table 1.

The overall structure of human ALR2 folds into an eight-stranded α/β-barrel with the active site located at the C-terminal end of the barrel. The $NADP^+$ binding site is located adjacent to a hydrophobic active site pocket.[19–21] As observed in the previously determined 1.3 Å resolution crystal structure of ALR2 in complex with the 2*S*4*R* isomer,[18] the active site is occupied by a citrate molecule from the crystallization buffer which anchors the 2*S*4*R* molecule from its exocyclic amide group through a hydrogen bonding interaction (3.18 Å). In addition, there is a hydrogen bond between the exocyclic amide group of the 2*S*4*R* molecule and Trp20 (2.90 Å). Stereodiagram of the 2*S*4*R* isomer bound to the active site of ALR2 is presented in Figure 1.

Implications for the Inhibition Mechanism. The structure of ALR2 in complex with the 2*S*4*R* isomer refined at an ultrahigh resolution of 0.78 Å indicated that the inhibitor was bound outside the active site in a neutral state based on the observed experimental electron density corresponding to the hydrogen of the 1′-position nitrogen atom of the cyclic imide ring (Figure 2). In the case of the ALR2−Fidarestat complex the inhibitor was bound negatively charged at the 1′-position nitrogen atom interacting favorably with the protonated Nϵ2 atom of the catalytic His110 and the positively charged nicotinamide ring of the coenzyme (Scheme 1).[14] Both carbonyl groups on the cyclic imide ring were present within hydrogen bonding distances from the Nϵ1 of Trp111 and the OH of Tyr48 (2.79 and 2.63 Å, respectively) while the exocyclic amide group formed a hydrogen bond with main-chain nitrogen atom of Leu300 (2.95 Å). On the other hand, the neutral cyclic imide ring of the bound 2*S*4*R* isomer acts as a hydrogen bond donor through its protonated 1′-position nitrogen atom to a water molecule (2.67 Å) which in turn acts as a hydrogen bond donor to the main-chain carbonyl oxygen atom of Lys21 (2.40 Å) and the side-chain carboxylate of the Glu193 (2.61 Å) from a symmetry related molecule in the crystal structure (Figure 2).

The binding of Fidarestat and its 2*S*4*R* isomer to ALR2 in two different protonation states, with the catalytic His110 protonated at the Nϵ2 position in the case of Fidarestat, suggested an inhibition mechanism by cyclic imide inhibitors. As observed in the case of the bound 2*S*4*R* isomer, initially the inhibitor crosses the biological membrane as a neutral compound. Once bound to the enzyme's active site the inhibitor becomes negatively charged by donating a proton, making the catalytic His110 positively charged and the resulting favorable electrostatic interaction contributes to the tight inhibitor binding. It should be noted that molecular modeling calculations on the binding of substrates to ALR2 predicted the protonation of the Nϵ2 atom of the catalytic His110 and hence the important role for this residue in drug design studies.[22]

Experimental Section

Expression and Purification of Human ALR2. The open reading frame of the human ALR2 gene (Accession Gene Bank/EMBL Data Bank Number J05017) was amplified by PCR from cDNA[23] and cloned into T7 RNA polymerase-based vector pET15b (Novagen). Expression of hexahistidine tagged protein in *Escherichia coli* strain BL21 (DE3; Novagen) was induced by IPTG

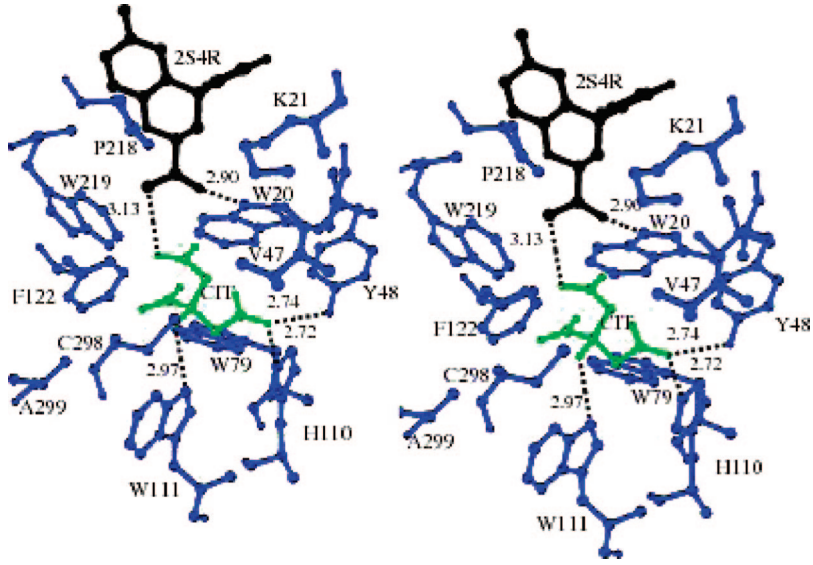

Figure 1. Stereodiagram showing 2*S*4*R* stereoisomer of Fidarestat (black) and citrate (green) bound to ALR2. Residues within 4 Å and hydrogen bonds as dashed lines with distances given in Å are shown. Figures were prepared using MOLSCRIPT.[31]

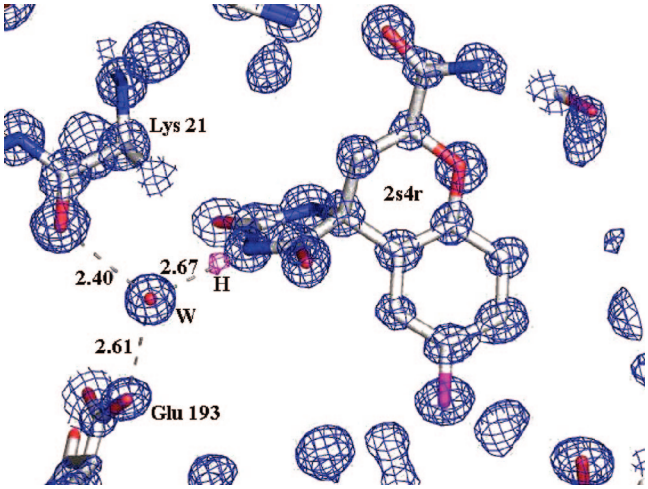

Figure 2. Model of the bound 2*S*4*R* isomer superimposed with $2F_o - F_c$ (blue) and F_o - F_c omit-H (magenta) σA-weighted electron density maps contoured at 2.0 σ cut-offs showing the position of the hydrogen atom on the inhibitor. Hydrogen bonding interactions between the water molecule, inhibitor, Lys21 and Glu193 are shown as dashed lines with distances given in Å. The electron density maps were calculated using diffraction data up to 0.78 Å resolution and contoured using Xtalview.[28]

(Euromedex) during a 3-h period at 37 °C. The pellet from a 4-L culture was disrupted by sonication and centrifuged. The supernatant was loaded onto a Talon metal-affinity column (Clonetech). After thrombin cleavage of the hexahistidine extension, the detagged protein was loaded onto a DEAE Sephadex A-50 column (Pharmacia) and eluted with a NaCl gradient.[23]

Crystallization. Before crystallization, human ALR2 at 16 mg/mL in 50 mM ammonium citrate buffer (pH 5) was mixed with $NADP^+$ and inhibitor (molar ratio of ALR2:$NADP^+$:inhibitor was 1:2:2.5). The ternary complex was crystallized using the vapor-diffusion method. The ALR2/$NADP^+$/inhibitor solution was mixed with an equal volume of 15% (w/v) polyethylene glycol (PEG) 6000 in 50 mM ammonium citrate buffer (pH 5) and 10 μL hanging droplets were placed above a well solution (1 mL) containing 20% PEG 6000 and 120 mM ammonium citrate. Crystals were grown at 277 K, transferred into a stabilization solution (25% PEG 6000), then into a cryoprotecting solution (40% PEG 6000) and dipped into liquid nitrogen. The crystallization pH for the ALR2−2*S*4*R* complex was same one used in the crystallization of the ALR2−Fidarestat complex.[14]

X-Ray Data Collection and Processing. The ternary complex with the bound 2*S*4*R* isomer crystallized in the monoclinic *P*21 space group, with unit cell parameters $a = 49.20$ Å, $b = 66.64$ Å, $c = 47.28$ Å, and $\beta = 91.67°$. There was one monomer per asymmetric unit, consisting of 316 amino acid residues. The solvent content was estimated to occupy 32.1% of the unit cell volume.[24] Almost complete synchrotron data set was collected at a temperature of 15 K (helium gas cryostat) at the APS beamline 19-ID from a 2*S*4*R* isomer complexed ALR2 flash-cooled crystal and processed using the programs *HKL2000* and SCALEPACK.[25] The exposure time (1–15 s), oscillation range (0.2–1°) and crystal-detector distance (115 mm) were adjusted to optimize the data set. The crystal proved resistance to radiation damage at 15 K, allowing the measurements of 2 × 180° zones in reciprocal space for a near complete data set between low- and high-resolution ranges. Data collection and processing statistics are shown in Table 1.

Structural Refinement. The atomic coordinates of the human ALR2−Fidarestat complex (PDB entry code 1PWM), which crystallized in the same space group with similar unit cell parameters, were used to solve the structure of the ternary complex with the bound 2*S*4*R* isomer. Crystallographic refinement involved repeated cycles of conjugate gradient energy minimization and temperature factor refinement.[26] Amino acid side-chains were fitted into $2F_o - F_c$ and $F_o - F_c$ electron density maps. The final $F_o - F_c$ map indicated clear electron density for the 2*S*4*R* isomer, where the citrate molecule was located bound into the active site. Water molecules were fitted into difference maps, anisotropic conjugate gradient refinement was conducted using the SHELX program package,[27] and in the final cycles riding H-atoms were introduced. The programs XtalView/Xfit[28] and Coot[29] were used for fitting the models into the electron density. The difference electron density maps allowed the identification of the H-atom on the 1′-position nitrogen of the inhibitor's cyclic imide ring together with multiple conformations for several amino acid residue side-chains. Low B-factors of bound inhibitors, partly due to helium cooling, recently have been associated with the visualization of their hydrogen atoms.[30] Refinement statistics are presented in Table 1.

The atomic coordinates have been deposited in the Protein Data Bank (ID code 3BCJ) and will be released immediately upon publication.

Acknowledgment. We thank Drs. Connie Darmanin and Tatiana Petrova for their help during the refinement process. This work was supported by the Centre National de la Recherche

Scientifique (CNRS), the Institut National de la Santé et de la Recherche Médicale, and the Hôpital Universitaire de Strasbourg (H.U.S). We acknowledge the use of 19-ID beamline at the Structural Biology Center/Advanced Photon Source supported by the U.S. Department of Energy, Office of Biological and Environmental Research, under Contract DE-AC02-06CH11357. This work was supported in part by the U.S. Department of Energy under Contract No. DE-AC02-05CH11231.

References

(1) Jez, J. M.; Bennet, M. J.; Schlegel, B. P.; Lewis, M.; Penning, T. M. Comparative anatomy of the aldo-keto reductase superfamily. *Biochem. J.* **1997**, *326*, 625–636.

(2) Warren, J. C.; Murdock, G. L.; Ma, Y.; Goodman, S. R.; Zimmer, W. E. Molecular cloning of testicular 20alpha-hydroxysteriod dehydrogenase: identity with aldose reductase. *Biochemistry* **1993**, *32*, 1401–1406.

(3) Jeffery, J.; Jornvall, H. Sorbitol dehydrogenase. *Adv. Enzymol. Relat. Areas Mol. Biol.* **1988**, *61*, 47–106.

(4) King, G. L.; Brownlee, M. B. The cellular and molecular mechanisms of diabetic complications. In *Endocrinology and Metabolism Clinics of North America*; Brownlee, M. B., King, G. L., Eds.; WB Saunders: Philadelphia, PA, 1996; Vol *25*, pp 255-270.

(5) Cameron, N. E.; Cotter, M. A.; Hohman, T. C. Interacrions between essential fatty acid, prostanoid, polyol pathway and nitric oxide mechanisms in the neurovascular deficit of diabetic rats. *Diabetologia* **1996**, *39*, 172–182.

(6) Lee, A. Y. W.; Chung, S. S. M. Contributions of polyol pathway to oxdidative stress in diabetic cataract. *FASEB J.* **1999**, *13*, 23–30.

(7) Chan, N. N.; Vallance, P.; Colhun, H. M. Nitric oxide and vascular responses in Type 1 diabetes. *Diabetologia* **2000**, *43*, 137–147.

(8) Wrobel, J.; Millen, J.; Sredy, J.; Dietrich, A.; Gorham, B. J.; Malamas, M.; Kelly, J. M.; Bauman, J. G.; Harrison, M. C.; Jones, L. R.; Guinosso, C.; Sestanj. Syntheses of tolrestat analogues containing additional substituents in the ring and their evaluation as aldose reductase inhibitors. Identification of potent, orally active 2-fluoro derivatives. *J. Med. Chem.* **1991**, *34*, 2504–2520.

(9) Yamagishi, M.; Yamada, Y.; Ozaki, K.; Asao, M.; Shimizu, R.; Suzuki, M.; Matsumoto, M.; Matsuoka, Y.; Mataumoto, K. Biological activities and quantitative structure−activity relationships of spiro[imidazolidine-4,4′(1′*H*)-quinazoline]-2,2′,5(3*H*0-triones as aldose reductase inhibitors. *J. Med. Chem.* **1992**, *35*, 2085–2094.

(10) Costantino, L.; Rastelli, G.; Vianello, P.; Cignarella, G.; Barlocco, D. Diabetes complications and their potential prevention: aldose reductase inhibition and other approaches. *Med. Res. Rev.* **1999**, *19*, 3–23.

(11) Mylari, B.; Larson, E.; Beyer, T.; Zembrowski, W.; Aldinger, C.; Dee, M.; Siegel, T.; Singletont, D. Novel, potent aldose reductase Inhibitors: 3,4-Dihydro-4-oxo-3-{[5-(trifluoromethyl)-2-benzothiazolyl]methyl}-1-phthalazineacetic acid (Zopolrestat) and congeners. *J. Med. Chem.* **1991**, *34*, 108–122.

(12) Kaul, C.; Ramarao, P. The role of aldose reductase inhibitors in diabetic complications: Recent trends. *Methods Find. Exp. Clin. Pharmacol.* **2001**, *23*, 465–475.

(13) Miyamoto, S. Recent advances in aldose reductase inhibitors: Potential agents for the treatment of diabetic complications. *Expert Opin. Ther. Pat.* **2002**, *12*, 621–631.

(14) El-Kabbani, O.; Darmanin, C.; Schneider, T. R.; Hazemann, I.; Ruiz, F.; Oka, M.; Joachimiak, A.; Schulze-Briese, C.; Tomizaki, T.; Mitschler, A.; Podjarny, A. Ultrahigh resolution drug design. II. Atomic resolution structures of human aldose reductase holoenzyme complexed with fidarestat and minalrestat: Implications for the binding of cyclic imide inhibitors. *Proteins* **2004**, *55*, 805–813.

(15) Malamas, M. S.; Hohman, T. C.; Milen. Novel spirosuccinimide aldose reductase inhibitors derived from isoquinoline-1,3-diones:2[(4-bromo-2-fluorophenyl)methyl]-6-fluorospiro[isoquinoline-4(1*H*),3′-pyrrolidine]-1,2′,3,5′(2*H*)-tetrone and congeners. *J. Med. Chem.* **1994**, *37*, 2043–2058.

(16) Malamas, M. S.; Hohman, T. C. N-substituted spirosuccinimide, spiropyridazine, spiroazetidine and acetic acid aldose reductase inhibitors derived from isoquinoline-1, 3-diones. *J. Med. Chem.* **1994**, *37*, 2059–2070.

(17) Negoro, T.; Murata, M.; Ueda, S.; Fujitani, B.; Ono, Y.; Kuromiya, A.; Komiya, M.; Suzuki, K.; Matsumoto, J. Novel, highly potent aldose reductase inhibitors: *R*-(−)-2-(4-bromo-2-fluorobenzyl)-1,2,3,4-tetrahydropyrrolo[1,2-*a*]pyrazine-4-spiro-3′-pyrolidine-1,2′,3,5-tetrone (AS-3201) and its congeners. *J. Med. Chem.* **1998**, *41*, 4118–4129.

(18) El-Kabbani, O.; Darmanin, C.; Oka, M.; Schulze-Briese, C.; Tomizaki, T.; Hazemann, I.; Mitschler, A.; Podjarny, A. High-resolution structures of human aldose reductase holoenzyme in complex with stereoisomers of the potent inhibitor Fidarestat: Stereospecific interaction between the enzyme and a cyclic imide type inhibitor. *J. Med. Chem.* **2004**, *47*, 4530–4537.

(19) Rondeau, J. M.; Tête-Favier, F.; Podjarny, A.; Reymann, J. M.; Barth, P.; Biellmann, J. F.; Moras, D. Novel NADPH-binding domain revealed by the crystal structure of aldose reductase. *Nature* **1992**, *355*, 469–472.

(20) El-Kabbani, O.; Wilson, D.; Petrash, J. M.; Quiocho, F. A. Structural features of the aldose reductase and aldehyde reductase inhibitor-binding sites. *Mol. Vision* **1998**, *4*, 19–25.

(21) Urzhumtsev, A.; Tête-Favier, F.; Mitschler, A.; Barbanton, J.; Barth, P.; Urzhumtseva, J. F.; Biellmann, A. D.; Podjarny, A.; Moras, D. A. 'Specificity' pocket inferred from the crystal structures of the complexes of aldose reductase with the pharmaceutically important inhibitors tolrestat and sorbinil. *Structure* **1997**, *5*, 601–612.

(22) De Winter, H. L.; von Itzstein, M. Aldose reductase as a target for drug design: Molecular modeling calculations on the binding of acyclic sugar substrates to the enzyme. *Biochemistry* **1995**, *34*, 8299–8308.

(23) Chung, S.; La Mendola, J. Cloning and sequence determination of human placental aldose reductase gene. *J. Biol. Chem.* **1989**, *264*, 4775–14777.

(24) Matthews, B. W. Solvent content of protein crystals. *J. Mol. Biol.* **1968**, *33*, 491–497.

(25) Otwinowski, Z.; Minor, W. Processing of X-ray diffraction data collected in oscillation mode. *Methods Enzymol.* **1997**, *276*, 307–326.

(26) Brünger, A. T.; Krukowski, A.; Erickson, J. W. Slow-cooling protocols for crystallographic refinement by simulated annealing. *Acta Crystallogr., Sect. A: Found. Crystallogr.* **1990**, *46*, 585–593.

(27) Sheldrick, G.; Schneider, T. SHELXL: High-resolution refinement. *Methods Enzymol.* **1997**, *277*, 319–343.

(28) McRee, D. E. XtalView/Xfit—A versatile program for manipulating atomic coordinates and electron density. *J. Struct. Biol.* **1999**, *125*, 156–165.

(29) Emsley, P.; Cowtan, K. Coot: model-building tools for molecular graphics. *Acta Crystallogr., Sect. D: Biol. Crystallogr.* **2004**, *60*, 2126–2132.

(30) Petrova, T.; Ginell, S.; Mitschler, A.; Hazemann, I.; Schneider, T.; Cousido, A.; Lunin, V. Y.; Joachimiak, A.; Podjarny, A. Ultrahigh-resolution study of protein atomic displacement parameters at cryotemperatures obtained with a helium cryostat. *Acta Crystallogr., Sect. D: Biol. Crystallogr.* **2006**, *62*, 1535–44.

(31) Kraulis, P. J. MOLSCRIPT: A program to produce both detailed and schematic plots of protein structures. *J. Appl. Crystallogr.* **1991**, *24*, 946–950.

JM701514K